LETTER

https://doi.org/10.1038/s41586-019-1008-7

Broadband electro-optic frequency comb generation in a lithium niobate microring resonator

Mian Zhang[1,2,7], Brandon Buscaino[3,7], Cheng Wang[1,4,7], Amirhassan Shams-Ansari[1,5], Christian Reimer[1,2], Rongrong Zhu[1,6], Joseph M. Kahn[3]* & Marko Lončar[1]*

Optical frequency combs consist of equally spaced discrete optical frequency components and are essential tools for optical communication, precision metrology, timing and spectroscopy[1–9]. At present, combs with wide spectra are usually generated by mode-locked lasers[10] or dispersion-engineered resonators with third-order Kerr nonlinearity[11]. An alternative method of comb production uses electro-optic (EO) phase modulation in a resonator with strong second-order nonlinearity, resulting in combs with excellent stability and controllability[12–14]. Previous EO combs, however, have been limited to narrow widths by a weak EO interaction strength and a lack of dispersion engineering in free-space systems. Here we overcome these limitations by realizing an integrated EO comb generator in a thin-film lithium niobate photonic platform that features a large EO response, ultralow optical loss and highly co-localized microwave and optical fields[15], while enabling dispersion engineering. Our measured EO comb spans more frequencies than the entire telecommunications L-band (over 900 comb lines spaced about 10 gigahertz apart), and we show that future dispersion engineering can enable octave-spanning combs. Furthermore, we demonstrate the high tolerance of our comb generator to modulation frequency detuning, with frequency spacing finely controllable over seven orders of magnitude (10 hertz to 100 megahertz), and we use this feature to generate dual-frequency combs in a single resonator. Our results show that integrated EO comb generators are capable of generating wide and stable comb spectra. Their excellent reconfigurability is a powerful complement to integrated Kerr combs, enabling applications ranging from spectroscopy[16] to optical communications[8].

The migration of optical frequency comb generators to integrated devices is motivated by a desire for efficient, compact, robust, and high-repetition-rate combs[11]. At present, almost all on-chip frequency comb generators rely on the Kerr (third-order, $\chi^{(3)}$) nonlinear optical process, in which a continuous-wave laser source excites a low-loss optical microresonator having a large Kerr nonlinear coefficient. This approach has enabled demonstration of wide-spanning Kerr frequency combs from the near- to mid-infrared portions of the spectrum in many material platforms, such as silicon, silicon dioxide, silicon nitride and magnesium fluoride[17–22]. Owing to the complex nature of the parametric oscillation process, however, the formation dynamics and noise properties of the Kerr combs are not yet fully understood and are still under active investigation[23,24]. Sophisticated control protocols are typically required to keep Kerr combs stabilized.

An alternative frequency-comb-generation method uses the EO effect in materials with second-order ($\chi^{(2)}$) nonlinearity. Conventionally, EO frequency-comb generators pass a continuous-wave laser through a sequence of discrete phase and amplitude modulators[25]. Such EO comb generators can feature remarkable comb power and flat spectra, and can support flexible frequency spacing. They usually have a narrow frequency span, however, comprising only tens of lines and spanning only a few nanometres[25–27]. Therefore, highly nonlinear fibre is typically required to broaden the comb spectrum further, increasing the system complexity and size[13]. Broader EO combs can be generated using an optical resonator to increase the nonlinear EO interaction strength[12,28]. In a canonical resonator-based EO comb generator, a continuous-wave laser is coupled to a bulk nonlinear crystal resonator containing an EO phase modulator (Fig. 1a), and comb lines are generated solely through the $\chi^{(2)}$ process. When the modulation frequency matches a harmonic of the resonator free spectral range (FSR), the optical sidebands generated by the phase modulator are resonant. In a low-loss resonator, the light passes through the modulator many times before being dissipated or coupled out, efficiently generating many comb lines spaced at the modulation frequency (Fig. 1b). The output frequency comb can be predicted accurately by closed-form solutions[28] with spacings equal to the modulation frequency. The overall flatness of the comb strongly depends on the round-trip modulation strength and the optical resonator loss. In particular, at frequencies away from the pump frequency, the comb line power decreases exponentially: the optical power in the qth comb line is $P_q \propto e^{-\frac{|q|l}{\beta}}$, where $\beta = V_p / V_\pi$ is the phase modulation index, V_p is the microwave drive peak amplitude, V_π is the half-wave voltage of the phase modulator, $l = \frac{2\pi\kappa}{\mathrm{FSR}}$ is the round-trip power loss coefficient of a resonator with damping rate $\kappa = \frac{\omega_0}{Q}$, Q is the resonator quality factor, and ω_0 is the optical frequency. It is therefore clear that strong phase modulation (large β) and a high-Q optical resonator (small l) are crucial for generating flat and broad EO combs. Furthermore, dispersion sets a fundamental limit on the total comb bandwidth by introducing frequency-dependent phase shifts that cause comb lines far from the pump frequency to fall out of resonance (see Methods). Although EO frequency combs generated by free-space or fibre-based optical cavities have been designed and extensively studied for over 25 years[12,28,29], practical comb widths are still limited to a few tens of nanometres by a combination of weak modulation and limited dispersion engineering[29].

Here we overcome these limitations of traditional discrete-component-based implementations by monolithically integrating an EO comb generator on a thin-film lithium niobate nanophotonic platform. Leveraging the large $\chi^{(2)}$ nonlinearity, strong microwave and optical field overlap, and ultralow-loss optical waveguides enabled by this platform, we demonstrate integrated EO combs with performance superior to bulk EO comb generators. Our devices feature an increase in comb width of nearly two orders of magnitude compared to previous integrated EO combs[30,31] based on indium phosphide and silicon platforms, where the effective EO modulation processes, created either by doping (silicon) or operating near the material's absorption band edge (indium phosphide), induce high optical losses.

[1]John A. Paulson School of Engineering and Applied Sciences, Harvard University, Cambridge, MA, USA. [2]HyperLight Corporation, Cambridge, MA, USA. [3]Edward L. Ginzton Laboratory, Department of Electrical Engineering, Stanford University, Stanford, CA, USA. [4]Department of Electronic Engineering and State Key Laboratory of Terahertz and Millimeter Waves, City University of Hong Kong, Hong Kong, China. [5]Department of Electrical Engineering and Computer Science, Howard University, Washington, DC, USA. [6]The Electromagnetics Academy at Zhejiang University, College of Information Science and Electronic Engineering, Zhejiang University, Hangzhou, China. [7]These authors contributed equally: Mian Zhang, Brandon Buscaino, Cheng Wang. *e-mail: jmk@ee.stanford.edu; loncar@seas.harvard.edu

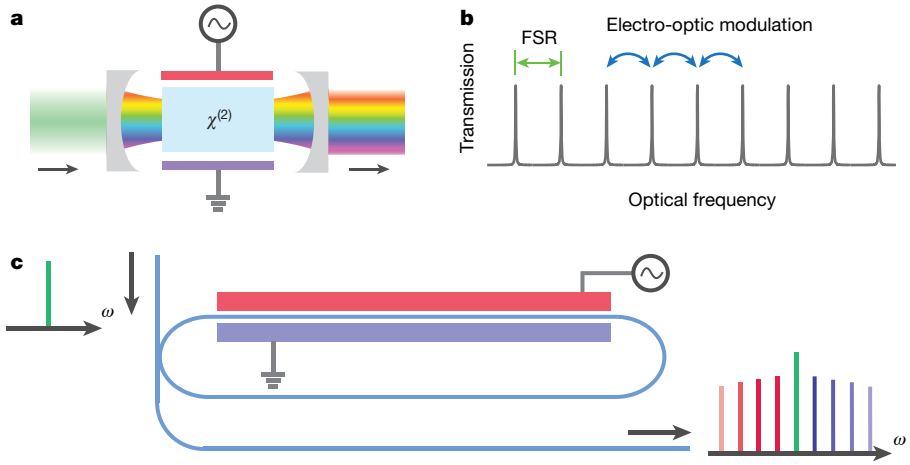

Fig. 1 | Resonator-enhanced EO comb generator. a, Schematic of a canonical EO comb generator comprising an EO ($\chi^{(2)}$) phase modulator inside a Fabry–Pérot resonator. A continuous-wave laser is coupled into the resonator and an optical frequency comb is generated at the output. **b**, EO comb generation principle. A microwave signal, with modulation frequency equal to the FSR of the optical resonator, couples light between different resonator modes. As a result, the input-coupled continuous-wave light is modulated, giving rise to sidebands at the modulation frequency, which are then recirculated to be modulated again. The modulation index determines the strength of coupling between nearby frequency components after passing through the modulator. **c**, Integrated microring EO comb generator. The Fabry–Pérot resonator can be replaced by a microring resonator that is EO-modulated at a frequency matching the FSR of the ring. Similarly to the Fabry–Pérot resonator, a continuous-wave laser coupled into the ring resonator is converted to a frequency comb in the output optical waveguide.

We demonstrate an EO frequency comb with over 900 unique frequencies spaced by 10.453 GHz, spanning 80 nm over part of the telecommunication C-band, the entire L-band and part of the U-band (Fig. 2). Our comb generator uses a low-loss lithium niobate microring resonator with loaded $Q \approx 1.5$ million, which is integrated with microwave electrodes for efficient phase modulation[15] via the strong second-order nonlinearity of lithium niobate ($r_{33} = 30$ pm V^{-1}) (Fig. 2a). Importantly, the tight confinement of the light (waveguide width, 1.4 μm) allows for gold electrodes to be placed only 3.3 μm away from the edge of the resonator, resulting in efficient microwave delivery to achieve strong phase modulation while not affecting the resonator Q factor. The two microwave electrodes are driven so that the top and bottom sections of the resonator experience opposite phase shifts, enabling phase matching between the microwave and the circulating optical field. The microresonator is modulated by an external microwave synthesizer with peak voltage $V_p = 10$ V ($\beta = 1.2\pi$) at a frequency

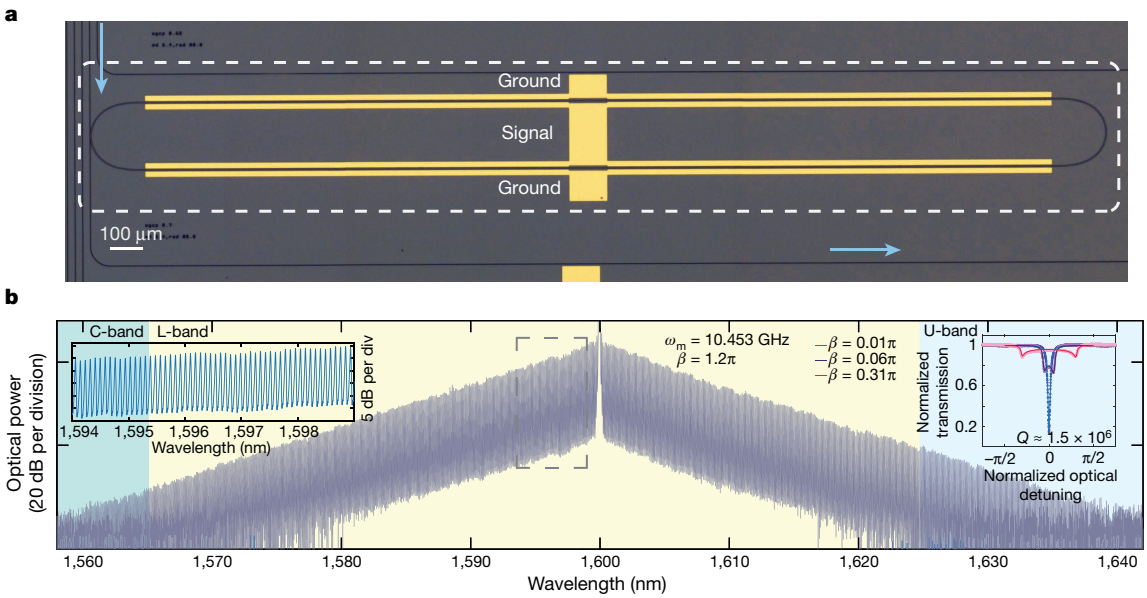

Fig. 2 | Integrated EO comb generator. a, Micrograph of a fabricated lithium niobate microring resonator (a shorter device is shown here for illustration purposes; see Methods). The black lines are etched optical waveguides and the yellow regions are gold microelectrodes. The gold electrodes are driven so that the phase shifts on the two sides of the microresonator are opposite, which is required to break the symmetry of different azimuthal order optical modes, enabling efficient frequency conversion. **b**, Measured output spectrum of the EO comb generated from the microring resonator, demonstrating a bandwidth exceeding 80 nm and more than 900 comb lines with a slope of 1 dB nm^{-1}. The input optical power is 2 mW and the microwave peak driving amplitude is $V_p = 10$ V. We note that the signal-to-noise ratio of the comb lines exceeds 40 dB but is limited by the noise floor and resolution of the optical spectrum analyser. The left inset shows a magnified view of several comb lines, with a line-to-line power variation of about 0.1 dB. The right inset shows the measured transmission spectrum for several different modulation indices β. When the modulation is turned on, the optical resonance is broadened by twice the modulation index. This behaviour is predicted well by the round-trip phase model (see Methods).

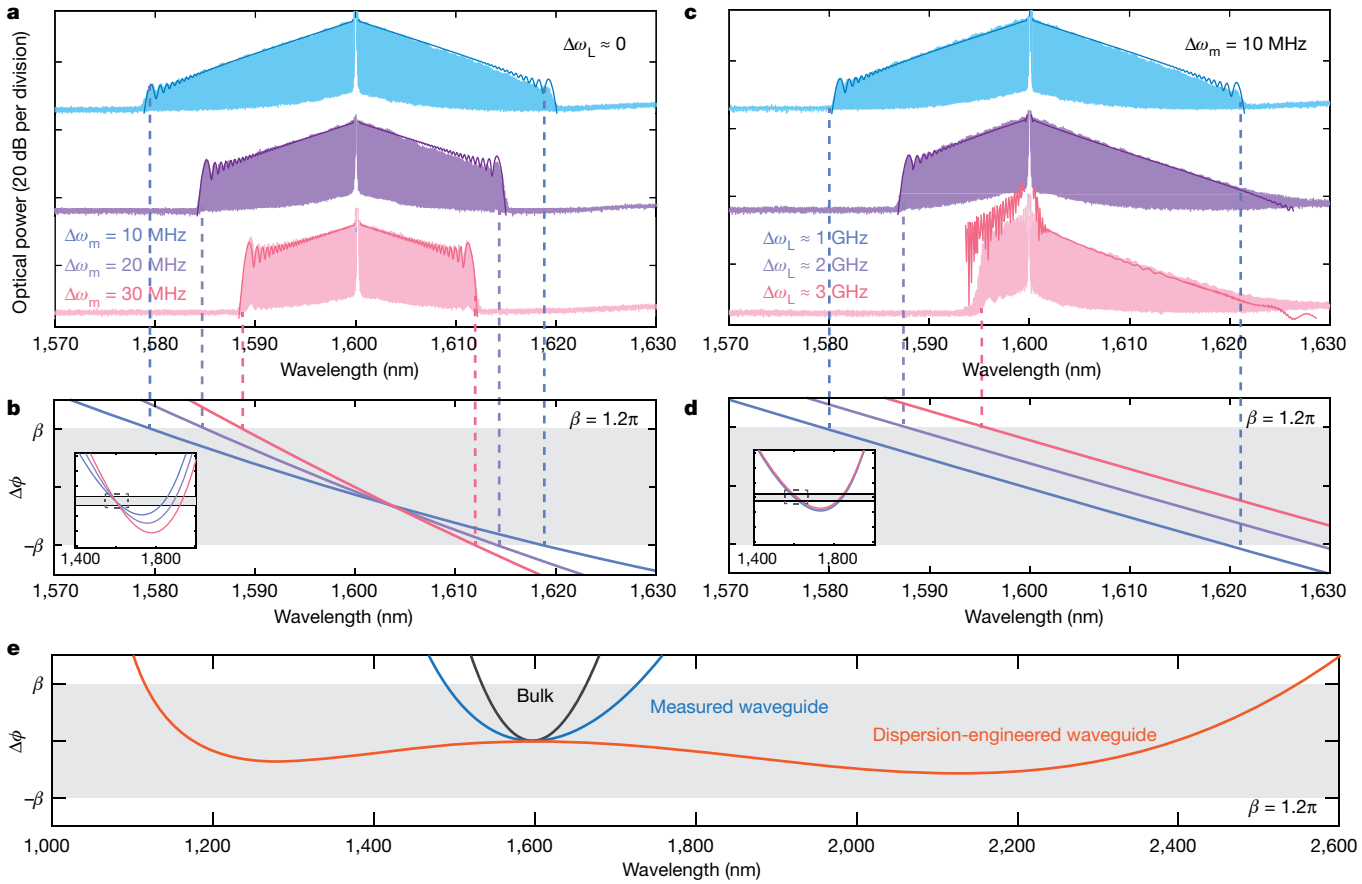

Fig. 3 | Controllability of the EO comb spectrum. a, Measured EO comb output spectrum (light, shaded) for various values of modulation frequency detuning from the resonator free spectral range ($\Delta\omega_m$). Numerical simulation of the comb envelopes (dark, lines, see Methods) match the measured spectra. **b**, Calculated round-trip phase $\Delta\phi$ versus wavelength for the modulation frequency detuning values shown in **a**. The grey-shaded region highlights the constructive interference condition region beyond which EO comb generation is suppressed. This region is bounded by $\pm\beta$, the round-trip modulation index. Insets show a zoomed-out view of the round-trip phase versus wavelength. The calculated cut-off frequency matches well with experimental data, as shown by the dashed lines extending to **a**. **c**, **d**, Measured and simulated comb spectrum and round-trip phase versus wavelength in the presence of both optical ($\Delta\omega_L$) and microwave detuning. Different comb shapes, such as a single-sided EO comb, can be generated. **e**, Simulated round-trip phase versus wavelength for traditional bulk devices (black), the measured integrated device (blue) and dispersion-engineered integrated devices (orange). The simulations demonstrate that integrated EO combs can achieve larger dispersion-limited bandwidths than devices based on bulk crystals and dispersion engineering can enable octave-spanning EO combs.

near the resonator FSR, and the generated comb spectrum (Fig. 2b) is well predicted by theory (see Methods). The comb spectrum has a slope of about 1 dB nm^{-1} (left inset in Fig. 2b), corresponding to power variation of less than 0.1 dB between adjacent comb lines. The comb lines have a signal-to-noise ratio of greater than 40 dB near the pump frequency, where the measurement is limited by the noise floor and the bandwidth of the optical spectrum analyser of resolution 20 pm.

We develop a theoretical model to quantify the fundamental limits of the wide spanning EO combs generated on our integrated platform. Traditional EO comb span is limited to a narrow width by a combination of weak microwave modulation strength and native material dispersion, which hinders the constructive interference needed for cascaded frequency conversion to generate comb lines far from the pump frequency[29]. In contrast, the integrated EO comb generators feature large modulation strength and the ability to engineer dispersion, which enables broader EO comb generation. To understand the limitations of the EO comb generation process, we look at the resonance condition for the qth comb line at optical frequency ω_q. In a traditional resonator, the round-trip constructive interference condition is $|\Delta\phi_q| < l/2$, where $\Delta\phi_q = \omega_q T - 2\pi N$ is the accumulated round-trip phase, T is the round-trip time and N is the number of optical cycles per round-trip (chosen to minimize $|\Delta\phi_q|$). For optical frequencies that satisfy this condition, the optical field interferes constructively within the resonator. When the resonator length is modulated, as in an EO comb generator, the resonance condition is modified into a dynamic one, where constructive interference occurs periodically at the microwave modulation frequency ω_m inside the resonator (that is, $|\Delta\phi_q + \beta\sin\omega_m t| < l/2$). Any frequency that does not satisfy this dynamic resonance condition will halt the frequency conversion process, thus limiting the comb width. This condition is reflected in the measured transmission spectrum of a microring resonator under microwave modulation (right inset in Fig. 2b). With no microwave modulation ($\beta \approx 0$), the transmission spectrum exhibits a Lorentzian shape. By contrast, when the electrodes are strongly modulated (large β), the half-width at half-maximum of the transmission spectrum broadened by a factor of approximately β, confirming that the tolerable absolute accumulated phase $|\Delta\phi_q|$ is increased to β. It is therefore clear that it is the strong phase modulation achieved in our EO comb generator that allows for the continued cascade of phase modulation even in the presence of dispersion.

To verify the round-trip phase model experimentally, we detune the optical and microwave frequencies to generate different comb shapes and widths. By increasing the microwave detuning up to 30 MHz (Fig. 3a), we observe a substantial reduction in the comb frequency span, which is predicted well by the round-trip phase model (Fig. 3b). Any frequency components having total accumulated phases larger than β cannot resonate, thus limiting the comb bandwidth. Taking advantage of this well understood dynamic resonance condition, we

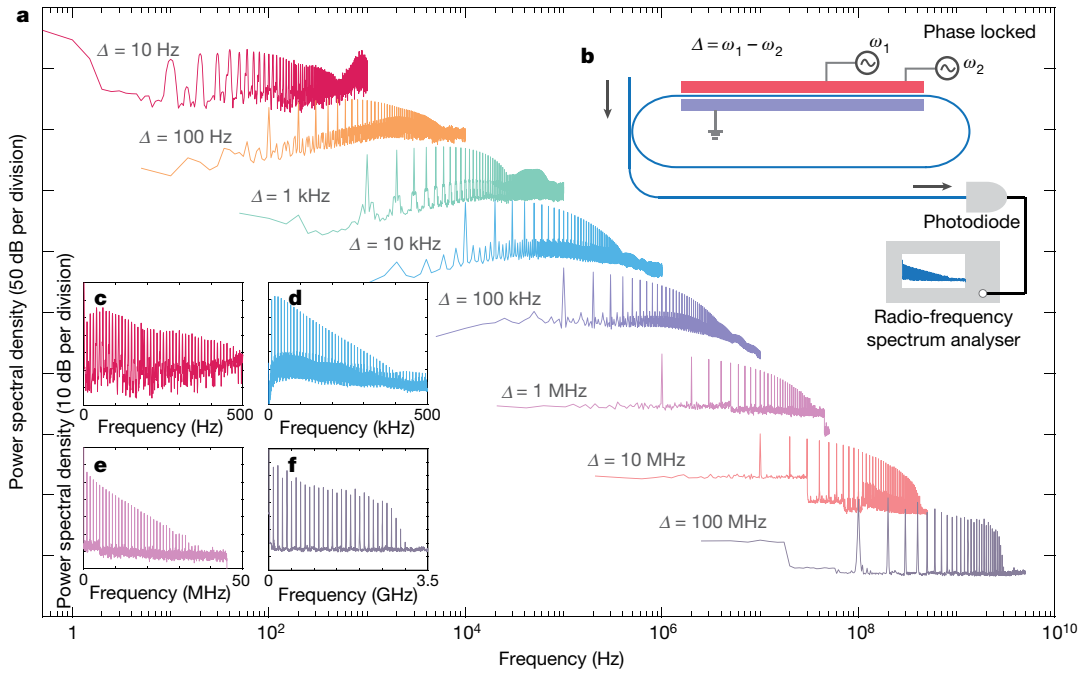

Fig. 4 | Dual-tone EO comb generation a, Demonstration of coherent beating of the EO comb. The measured beat-note power spectral density is shown on a logarithmic scale to highlight the flexibility in the control of the EO comb spacing over seven orders of magnitude, from 10 Hz to 100 MHz. **b**, Experimental setup. The EO comb generator is driven by a superposition of two phase-locked microwave signals with various values of frequency offset Δ. The optical output is detected by a fast photodiode, and the beat notes are detected by a radio-frequency spectrum analyser. **c**–**f**, Magnification of the individual beat notes for various comb spacings on a linear frequency scale. This measurement, which demonstrates frequency components well beyond the resonator bandwidth in the absence of modulation, confirms that phase modulation changes the resonance condition to tolerate large microwave detuning. Additionally, this measurement demonstrates the extreme flexibility in comb frequency spacing for practical applications such as dual-comb spectroscopy or comb-based ranging.

can generate asymmetric combs by appropriately choosing the optical and microwave detuning (Fig. 3c, d). EO combs driven off resonance, such as this one, could be used as low-noise sources for optical communications owing to the noise-filtering properties of the optical resonator[32] (see Methods).

The ability to engineer the dispersion of integrated EO comb generators could allow achievable comb bandwidth over a full octave. Traditionally, the span of EO comb generators is restricted by the dispersion of bulk materials, whereas our EO comb generators tightly confine light in optical waveguides, enabling fine-tuning of dispersion. Our simulation shows that, using a higher microwave modulation frequency of 50 GHz, a higher optical pump power (currently only 2 mW in our experiment), and a dispersion-engineered lithium niobate rib waveguide resonator that minimizes variation in FSR, it will be possible to generate an EO comb spanning over an octave (Fig. 3e and Methods).

Perhaps the most attractive properties of EO comb generators are their excellent configurability and stability. Leveraging the high tolerance to the detuning of the modulation frequency from the resonator FSR, we drive the microresonator electrodes with two phase-locked microwave sources at various frequency offsets from 10.453 GHz, spanning over seven orders of magnitude, ranging from 10 Hz to over 100 MHz. The comb generator is optically pumped close to zero detuning at a resonance near 1,600 nm and the output of the comb generator is then connected to a high-speed photodetector, allowing observation of coherent beating between comb lines (Fig. 4). Owing to the strong phase modulation, this dual-driven EO comb contains frequency components far beyond the ring resonator linewidth without modulation (120 MHz). The ability to vary the frequency spacing of resonator-based EO combs over seven orders of magnitude is in stark contrast with Kerr-based combs, whose frequency offset is predetermined by the fabricated resonator dimensions[5]. This flexibility in comb drive frequencies may enable applications requiring a reconfigurable dynamic range, such as dual-comb-based optical ranging[7,9] and spectroscopy[3–6]. Two independent microresonators can be integrated onto the same lithium niobate chip with high fabrication tolerance to avoid potential aliasing of the comb lines.

Our work using high-Q microring resonators and highly confined optical waveguides for EO comb generation is the first step towards a new generation of integrated EO comb sources. Our demonstration of an EO comb that is almost two orders of magnitude larger than prior integrated EO combs suggests that dispersion engineering and high-frequency modulation could soon enable octave-spanning EO comb generators. Importantly, the approach demonstrated here can be used to realize EO combs over the entire lithium niobate transparency window, including the visible and near-infrared portions of the spectrum, simultaneously. With the added ability to integrate filters and resonators adjacent to or inside EO comb generators on the same chip, the comb line power and hence the signal-to-noise ratio can be further increased[33] by nearly 20 dB. Our approach allows complex EO circuits to be integrated on the same chip and thus has the potential to transform microresonator frequency comb applications. For example, high-performance EO combs featuring high power and flat combs could enable terabit-per-second optical communications links that rely on stable, low-noise combs as sources for high-capacity wavelength-division multiplexed systems on a single chip[8]. Furthermore, the EO comb generator demonstrated in this work provides many stable coherent optical frequencies with electrically adjustable frequency spacing, paving the way for efficient dual-comb spectroscopy[3–6] on a chip or highly reconfigurable comb-based ranging[7,9].

Online content

Any methods, additional references, Nature Research reporting summaries, source data, statements of data availability and associated accession codes are available at https://doi.org/10.1038/s41586-019-1008-7.

Received: 5 August 2018; Accepted: 27 December 2018;
Published online 11 March 2019.

1. Ye, J., Schnatz, H. & Hollberg, L. W. Optical frequency combs: from frequency metrology to optical phase control. *IEEE J. Sel. Top. Quantum Electron.* **9**, 1041–1058 (2003).
2. Papp, S. B. et al. Microresonator frequency comb optical clock. *Optica* **1**, 10–14 (2014).
3. Coddington, I., Newbury, N. & Swann, W. Dual-comb spectroscopy. *Optica* **3**, 414–426 (2016).
4. Bernhardt, B. et al. Cavity-enhanced dual-comb spectroscopy. *Nat. Photon.* **4**, 55–57 (2010).
5. Dutt, A. et al. On-chip dual-comb source for spectroscopy. *Sci. Adv.* **4**, e1701858 (2018).
6. Suh, M.-G., Yang, Q.-F., Yang, K. Y., Yi, X. & Vahala, K. J. Microresonator soliton dual-comb spectroscopy. *Science* **354**, 600–603 (2016).
7. Trocha, P. et al. Ultrafast optical ranging using microresonator soliton frequency combs. *Science* **359**, 887–891 (2018).
8. Pfeifle, J. et al. Coherent terabit communications with microresonator Kerr frequency combs. *Nat. Photon.* **8**, 375–380 (2014).
9. Suh, M.-G. & Vahala, K. J. Soliton microcomb range measurement. *Science* **359**, 884–887 (2018).
10. Cundiff, S. T., Ye, J. & Hall, J. L. Optical frequency synthesis based on mode-locked lasers. *Rev. Sci. Instrum.* **72**, 3749–3771 (2001).
11. Kippenberg, T. J., Gaeta, A. L., Lipson, M. & Gorodetsky, M. L. Dissipative Kerr solitons in optical microresonators. *Science* **361**, eaan8083 (2018).
12. Kourogi, M., Nakagawa, K. & Ohtsu, M. Wide-span optical frequency comb generator for accurate optical frequency difference measurement. *IEEE J. Quantum Electron.* **29**, 2693–2701 (1993).
13. Beha, K. et al. Electronic synthesis of light. *Optica* **4**, 406–411 (2017).
14. Xiao, S., Hollberg, L., Newbury, N. R. & Diddams, S. A. Toward a low-jitter 10 GHz pulsed source with an optical frequency comb generator. *Opt. Express* **16**, 8498–8508 (2008).
15. Wang, C. et al. Integrated lithium niobate electro-optic modulators operating at CMOS-compatible voltages. *Nature* **562**, 101–104 (2018).
16. Millot, G. et al. Frequency-agile dual-comb spectroscopy. *Nat. Photon.* **10**, 27–30 (2016).
17. Del'Haye, P. et al. Octave spanning tunable frequency comb from a microresonator. *Phys. Rev. Lett.* **107**, 063901 (2011).
18. Okawachi, Y. et al. Octave-spanning frequency comb generation in a silicon nitride chip. *Opt. Lett.* **36**, 3398–3400 (2011).
19. Griffith, A. G. et al. Silicon-chip mid-infrared frequency comb generation. *Nat. Commun.* **6**, 6299 (2015).
20. Savchenkov, A. A. et al. Tunable optical frequency comb with a crystalline whispering gallery mode resonator. *Phys. Rev. Lett.* **101**, 093902 (2008).
21. Liang, W. et al. Generation of near-infrared frequency combs from a MgF_2 whispering gallery mode resonator. *Opt. Lett.* **36**, 2290–2292 (2011).
22. Gräupner, P., Pommier, J. C., Cachard, A. & Coutaz, J. L. Electro-optical effect in aluminum nitride waveguides. *J. Appl. Phys.* **71**, 4136–4139 (1992).
23. Herr, T. et al. Universal formation dynamics and noise of Kerr-frequency combs in microresonators. *Nat. Photon.* **6**, 480–487 (2012).
24. Yi, X. et al. Single-mode dispersive waves and soliton microcomb dynamics. *Nat. Commun.* **8**, 14869 (2017).
25. Metcalf, A. J., Torres-Company, V., Leaird, D. E. & Weiner, A. M. High-power broadly tunable electrooptic frequency comb generator. *IEEE J. Sel. Top. Quantum Electron.* **19**, 231–236 (2013).
26. Sakamoto, T., Kawanishi, T. & Izutsu, M. Asymptotic formalism for ultraflat optical frequency comb generation using a Mach-Zehnder modulator. *Opt. Lett.* **32**, 1515–1517 (2007).
27. Ozharar, S., Quinlan, F., Ozdur, I., Gee, S. & Delfyett, P. J. Ultraflat optical comb generation by phase-only modulation of continuous-wave light. *IEEE Photonics Technol. Lett.* **20**, 36–38 (2008).
28. Ho, K. P. & Kahn, J. M. Optical frequency comb generator using phase modulation in amplified circulating loop. *IEEE Photonics Technol. Lett.* **5**, 721–725 (1993).
29. Kourogi, M., Widiyatomoko, B., Takeuchi, Y. & Ohtsu, M. Limit of optical-frequency comb generation due to material dispersion. *IEEE J. Quantum Electron.* **31**, 2120–2126 (1995).
30. Dupuis, N. et al. InP-based comb generator for optical OFDM. *J. Lightwave Technol.* **30**, 466–472 (2012).
31. Demirtzioglou, I. et al. Frequency comb generation in a silicon ring resonator modulator. *Opt. Express* **26**, 790–796 (2018).
32. Kim, J., Richardson, D. J. & Slavík, R. Cavity-induced phase noise suppression in a Fabry–Perot modulator-based optical frequency comb. *Opt. Lett.* **42**, 1536–1539 (2017).
33. Kourogi, M., Enami, T. & Ohtsu, M. A coupled-cavity monolithic optical frequency comb generator. *IEEE Photonics Technol. Lett.* **8**, 1698–1700 (1996).

Acknowledgements This work is supported by the National Science Foundation (award numbers ECCS-1609549, ECCS-1740291 E2CDA, ECCS-1740296 E2CDA and DMR-1231319); the Harvard University Office of Technology Development (Physical Sciences and Engineering Accelerator Award); and Facebook, Inc. Device fabrication is performed at the Harvard University Center for Nanoscale Systems, a member of the National Nanotechnology Coordinated Infrastructure Network, which is supported by the National Science Foundation (award number ECCS-1541959).

Reviewer information *Nature* thanks Yanne K. Chembo, Paulina Kuo and the other anonymous reviewer(s) for their contribution to the peer review of this work.

Author contributions M.Z., B.B., C.W., J.M.K. and M.L. conceived the experiment. M.Z., C.W. and A.S.-A. designed and fabricated the devices. B.B. performed theoretical modelling and numerical simulations of the integrated EO comb. M.Z. and R.Z. designed waveguide dispersion. M.Z., C.W., A.S.-A. and C.R. carried out the device characterization. M.Z. and B.B. performed the data analysis. M.Z. and B.B. wrote the manuscript with contributions from all authors. J.M.K. and M.L. supervised the project.

Competing interests The authors declare competing interests: M.Z., C.W., C.R. and M.L. are involved in developing lithium niobate technologies at HyperLight Corporation.

Additional information
Extended data is available for this paper at https://doi.org/10.1038/s41586-019-1008-7.
Reprints and permissions information is available at http://www.nature.com/reprints.
Correspondence and requests for materials should be addressed to J.M.K. or M.L.
Publisher's note: Springer Nature remains neutral with regard to jurisdictional claims in published maps and institutional affiliations.

METHODS

Fabrication details. All devices are fabricated on x-cut single crystalline thin-film lithium niobate wafers (NANOLN). The wafer stack consists of a 600-nm thin-film lithium niobate layer, a 2-μm thermally grown SiO_2 layer and a 500-μm silicon handle layer. Standard electron-beam lithography is used to pattern optical waveguide and micro-racetrack resonators. The patterns are then transferred into the lithium niobate layer using argon (Ar^+) plasma etching in an inductively coupled plasma reactive ion etching (ICP-RIE) tool[34]. The etch depth is 350 nm, leaving a 250-nm-thick lithium niobate slab behind, which enables efficient electric field penetration into the waveguide core. Gold contact patterns are then created using aligned electron-beam lithography, and the metal is transferred using electron-beam evaporation methods and lift-off processes. The chip is then diced and the facets are polished for end-fire optical coupling. A 10-GHz FSR micro-racetrack measures 200 μm by 6.2 mm. For illustration purposes, a 25-GHz FSR ring with otherwise the same design measuring 200 μm by 2.7 mm is displayed in Fig. 2a, where the straight section has a reduced length.

Microwave driving circuitry. The 10-GHz microwave drive signal is generated by a radio-frequency synthesizer and amplified by an electrical power amplifier. The amplified electrical signal is passed through a microwave circulator and delivered to the microelectrodes. As the microelectrodes represent a capacitive load, most of the electrical driving signal is reflected back to the circulator and terminated at the circulator output by a 50-Ω load.

In the dual-drive EO comb generation experiment, two radio-frequency synthesizers are phase-locked via a common 10-MHz clock and are free to operate at different frequencies. The two sinusoidal microwave signals are power balanced and combined using a radio-frequency power splitter and passed through the amplifier-circulator circuitry.

Optical characterization and detection. Light from a tunable laser (SANTEC TS510) is launched into, and the comb output is collected from, the lithium niobate waveguides via a pair of lensed optical fibres. The output comb is passed to an optical spectrum analyser having a minimum resolution of 20 pm. This finite resolution accounts for the limited signal-to-noise ratio observed in Fig. 2b (about 20 dB). The shot-noise-limited signal-to-noise ratio is much higher, as the comb shot noise lies below the noise floor of the optical spectrum analyser. Although the measurement in the paper is chosen to centre at 1,600 nm, the frequency comb centre wavelength can be flexibly chosen between 1,500 nm to 1,680 nm of the tunable laser's range without affecting much of the generated comb width.

In the dual-drive EO comb measurements, the modulated light is passed to a fast photodetector (New Focus 1544A) and the resulting electrical signal is sent to a radio-frequency spectrum analyser to record the beating in the radio-frequency domain.

Measurement and calculation of resonator parameters. As demonstrated by equation (6) below, there are four resonator parameters that fully characterize the EO comb spectrum: the internal round-trip transmission coefficient α, the power coupling coefficient k, the coupler insertion loss of the coupler γ, and the phase modulation index β. Finding each of these four parameters by fitting to the comb spectrum of equation (6) is difficult because the output comb can be fully determined by a subset of these independent parameters (for example, increasing the modulation index has the same effect as decreasing the loss in the resonator). Instead, each of the parameters must be measured separately.

We find α and k by measuring the total transmitted power without phase modulation (right inset in Fig. 2b). By fitting to the expected transmission of an all-pass ring resonator, we find $Q = 1.5 \times 10^6$, $\alpha = 0.95$ and $k = 0.027$. Then we perform a grid search optimization for γ and β comparing the measured output spectrum (Fig. 2b) with the spectrum determined from the output time-domain electric field of equation (5) below. We find a best fit for $\gamma = -0.004$ dB and $\beta = 1.2\pi$, where the average difference between experimental and theoretical comb line power is 0.6 dB. The relative uncertainty in the measurement of β in this case is ±4%, calculated by finding the furthest fit within a 95% confidence interval and calculating the resulting value of β. The output power transmission for nonzero modulation indices (right inset in Fig. 2b) is calculated by sampling the output electric field with equation (5) and averaging the power over more than 100 modulation periods.

Dispersion engineering in thin-film lithium niobate waveguides. To achieve wide-spanning EO combs, the waveguide dispersion should be engineered such that the group velocity (or the FSR) of the ring is roughly constant across the entire frequency range. We simulate the dispersion of the waveguide using finite element methods (Lumerical Mode Solutions; https://www.lumerical.com/products/mode-solutions/). The simulation accounts for the lithium niobate material anisotropy and the finite waveguide etching angle (around 70° from horizontal). The round-trip phase of the light inside the resonator is calculated by integrating the simulated group velocity dispersion twice to determine the total frequency-dependent phase shift. For the device we demonstrate here, with a waveguide ridge height of 350 nm, waveguide width of 1.4 μm, slab thickness of 250 nm and SiO_2 top cladding of 1.5 μm, the dispersion of the waveguide is weakly normal and supports an EO comb cut-off bandwidth of about 250 nm. We find that for an air-clad waveguide with a 600-nm thin-film lithium niobate layer, etch depth of 550 nm and waveguide width of 1.8 μm, a comb spanning about 1.3 octaves can be generated with a round-trip modulation frequency of 50 GHz and strength of $\beta = 1.2\pi$, as shown in Fig. 3e. The waveguide dispersion can be tailored for low microwave drive powers at the expense of a smaller comb span. For an air-clad waveguide with a thin-film lithium niobate layer of 650 nm, etch depth of 620 nm and waveguide width of 2,400 nm, an octave-spanning comb can be generated with a phase-modulation strength of only $\beta = 0.3\pi$. These results are presented in Extended Data Fig. 1.

Microwave driver power consumption. The current EO comb generator features a direct capacitive drive electrode design, where the electrical power consumption P_E can be estimated as

$$P_E = \frac{1}{2} C V_p^2 \omega_m \tag{1}$$

where $C \approx 200$ fF is the estimated capacitance[35], V_p is the peak voltage and ω_m is the microwave frequency. For the broad comb shown in Fig. 2, the calculated electrical power consumption is about 630 mW.

There are several ways to reduce the electrical power consumption. At present the electrode gaps are not optimized and can be reduced to increase the EO efficiency directly. A microwave resonator with a quality factor of Q_m can be used to enhance the driving voltage dramatically, as only a narrow-band microwave source is required. A microwave resonator has an enhanced voltage $V_{p,\mathrm{eff}}$ of

$$V_{p,\mathrm{eff}} = \sqrt{\frac{2 P_E Q_m}{\omega_m C}} \tag{2}$$

Comparing equations (2) and (1), the effective pumping power is increased by a factor of Q_m. This means that for a moderate $Q_m = 20$ at 10 GHz, the power consumption can be reduced to about 30 mW.

To estimate the minimum electrical power required to generate an octave-spanning EO comb, we consider the first case where the resonator is driven to $\beta = 1.2\pi$ at 50 GHz FSR. Here the capacitance of the device is reduced by a factor of 5 as the ring resonator becomes smaller to achieve a 50 GHz FSR. At the same time, the V_π also increases by a factor of 5 owing to the shorter electrodes. For $Q_m = 20$, the calculated power consumption is about 750 mW. Through dispersion engineering and higher-Q optical microresonators, it is possible to achieve an octave-spanning EO comb even at low drive voltages of $V_p = 0.3 V_\pi$. In this case, the electrical power consumption is further reduced to only about 45 mW.

Canonical EO comb generator design. The concept of a comb generator using a resonator to enhance frequency generation by an EO phase modulator dates to 1972 (ref. [36]). Theoretical and experimental work[12,28] on these comb generators continued in the 1990s. Recent advances in low-loss integrated lithium niobate photonic platform[34] has motivated re-examination of these comb generators.

A canonical waveguide-based comb generator is shown in Fig. 1c. A single-frequency input with electric field $E_{in}(t) = \hat{E}_{in} e^{i\omega_0 t}$ is coupled, with power coupling coefficient k and insertion loss γ, to a resonator having round-trip time T at the centre frequency ω_0 and round-trip intrinsic power loss $1-\alpha$. The resonator contains a phase modulator driven with modulation index β and frequency ω_m. The output electric field is[28]

$$E_{out}(t) = \sqrt{(1-\gamma)(1-k)}\, E_{in}(t) - k\sqrt{\frac{1-\gamma}{1-k}} \sum_{n=1}^{\infty} r^n e^{-i\beta F_n(\omega_m t)} E_{in}(t - nT) \tag{3}$$

where $r = \sqrt{(1-\gamma)(1-k)\alpha}$ is the round-trip electric field transmission and $F_n(\omega_m t) = \sum_{i=1}^{n} \sin\omega_m(t - iT)$ is the modulator coherence function. The parameter $l = 1 - r^2$, corresponding to the round-trip power loss, is used in the main text for simplicity. When the optical carrier is resonant in the resonator ($\omega_0 T = 2\pi m_1$, where m_1 is an integer) and the microwave drive signal is resonant ($\omega_m T = 2\pi m_2$, where m_2 is an integer), the modulator coherence function becomes $F_n(\omega_m t) = n\sin\omega_m(t - iT)$ and the output electric field can be simplified to

$$E_{out}(t) = \left[\sqrt{(1-\gamma)(1-k)} - k\sqrt{\frac{1-\gamma}{1-k}}\, \frac{r\, e^{-i\beta\sin\omega_m t}}{1 - r\, e^{-i\beta\sin\omega_m t}}\right] E_{in}(t) \tag{4}$$

This output electric field corresponds to an optical frequency comb spaced at the modulation frequency. The power in the qth comb line away from the centre frequency can be found by rewriting equation (3) as

$$\begin{aligned} E_{out}(t) &= \sqrt{(1-\gamma)(1-k)}\, \hat{E}_{in}\, e^{i\omega_0 t} - k\sqrt{\frac{1-\gamma}{1-k}} \sum_{n=1}^{\infty} r^n e^{-i\beta n \sin\omega_m t} \hat{E}_{in}\, e^{i\omega_0(t)} \\ &= \sqrt{(1-\gamma)(1-k)}\, \hat{E}_{in}\, e^{i\omega_0 t} - k\sqrt{\frac{1-\gamma}{1-k}} \sum_{q=-\infty}^{\infty} \hat{E}_{in}\, e^{i(\omega_0 + q\omega_m)t} \sum_{n=1}^{\infty} r^n J_q(\beta n) \end{aligned} \tag{5}$$

where J_q is the qth-order Bessel function of the first kind. The power of the qth (nonzero) comb line is then

$$P_q = k^2 \frac{1-\gamma}{1-k} P_{\text{in}} \left| \sum_{n=1}^{\infty} r^n J_q(\beta n) \right|^2 \tag{6}$$

Ref. [12] found an approximation for the power of the qth comb: $P_q \propto e^{-\frac{|q|(1-r^2)}{\beta}}$.

In the presence of optical and microwave detuning from resonance, the comb spectrum can still be calculated. When the optical carrier is off resonance, the total round-trip phase is $\omega_0 T = 2\pi m_1 + \phi_{\text{opt}}$. Similarly, when the microwave carrier is off resonance the total round-trip phase is $\omega_m T = 2\pi m_2 + \phi_{\text{micro}}$. Using these expressions in equation (3), we can find the following expression for the power in the qth comb line:

$$P_q = k^2 \frac{1-\gamma}{1-k} P_{\text{in}} \left| \sum_{p=-\infty}^{\infty} \sum_{n=1}^{\infty} (r e^{i\phi_{\text{opt}}})^n e^{ip\frac{\pi}{2}} J_{q-p}(\beta_o(\phi_{\text{micro}}, n)) J_p(\beta_e(\phi_{\text{micro}}, n)) \right|^2 \tag{7}$$

The modified even and odd modulation indices (β_e and β_o, respectively) are

$$\beta_e(\phi_{\text{micro}}, n) = \beta \left\{ \frac{1}{2}\cot(\phi_{\text{micro}}/2) - \frac{\cos\left[(n+\frac{1}{2})\phi_{\text{micro}}\right]}{2\sin(\phi_{\text{micro}}/2)} \right\} \tag{8}$$

$$\beta_o(\phi_{\text{micro}}, n) = \beta \left\{ -\frac{1}{2} + \frac{\sin\left[(n+\frac{1}{2})\phi_{\text{micro}}\right]}{2\sin(\phi_{\text{micro}}/2)} \right\} \tag{9}$$

It is clear here that in the regime of low optical detuning, the slope of the comb decreases by a factor of $\cos(\phi_{\text{opt}})$. This effect has been studied and reported in ref. [37]. The effect of microwave detuning is harder to visualize, but results in a destructive interference condition for large values of q in equation (7). This effect is demonstrated experimentally and theoretically in Fig. 3a, b.

Noise properties. The optical phase noise of the comb lines is important in applications that require high optical signal-to-noise ratios, such as high-capacity optical communications. It is well known that the optical phase noise contribution from the pump laser does not increase with increasing comb line index[28]. By contrast, the phase noise contribution from the microwave modulation signal increases in power with the comb line quadratically with q. This can be shown by modifying the modulator coherence function to include the effects of microwave modulation phase noise $\theta(t)$:

$$F_n(\omega_m t) = \sum_{i=1}^{n} \sin\omega_m(t - iT + \theta(t - iT)) \tag{10}$$

The output optical field can then be written as:

$$E_{\text{out}}(t) = \sqrt{(1-\gamma)(1-k)}\,\hat{E}_{\text{in}} \\ e^{i\omega_0 t} - k\sqrt{\frac{1-\gamma}{1-k}}\,\hat{E}_{\text{in}} \sum_{q=-\infty}^{\infty} \sum_{n=1} r^n J_q(\beta n)\, e^{i(\omega_0 + q\omega_m)t + iq\theta(t)} \tag{11}$$

The phase noise amplitude increases linearly with increasing comb line index q, corresponding to a quadratic increase in phase noise power.

For applications that require few comb lines, this increase in microwave phase noise is often negligible because quartz crystal oscillators have very low phase noise. For applications requiring many comb lines, however, the effect of microwave phase noise may be noticeable. Recently, there has been experimental evidence of microwave phase noise suppression in EO comb generators[32,38]. In these studies, the phase noise of free-space resonator-enhanced EO combs is measured and simulated. When the optical and microwave frequencies are resonant, higher-order comb lines do not experience a quadratic increase in phase noise power. Instead, high-frequency phase noise components are attenuated such that the high-frequency phase noise is comparable for all comb lines. Furthermore, detuning the optical and microwave frequencies from the resonator FSR can further reduce the phase noise power. These experiments suggest that EO comb generators can generate low-noise comb lines over their entire dispersion-limited bandwidth. Additionally, integrated platforms, such as the one presented in the main text, enable additional filtering cavities and structures to be readily included in the resonator structure.

Round-trip phase model. To include the effect of dispersion, we introduce a round-trip phase model. In particular, we consider that the destructive interference that occurs due to the microwave detuning motivates a phase-based resonance approximation for the viable comb bandwidth. Previous analytical work[29] provided a mathematical treatment of the dispersion limits of resonator-based EO comb generators. Here, as a complement to that work, we clarify the physical interpretation of the round-trip phase model and demonstrate its application to combs of arbitrary bandwidth within a given dispersion-limited window.

The resonance condition of an optical frequency ω_q in a microresonator without EO modulation is $|\omega_q T - 2\pi N| < l/2$, where the total round-trip phase offset $\Delta\phi_q = \omega_q T - 2\pi N$, where $T = 1/\text{FSR}$, is the round-trip time and N is the number of optical cycles per round trip that ensures that $|\Delta\phi_q| < 2\pi$. Frequency components outside the resonance are attenuated by destructive interference, and thus do not resonate. When the resonance condition is satisfied, the optical fields constructively interfere inside the resonator at every time and spatial location.

In a resonator containing an EO phase modulator, the (now time-dependent) resonance condition becomes $|\Delta\phi_q + \beta\sin(2\pi f_m t)| < l/2$, where β is the modulation index and f_m is the modulation frequency. Here, it is clear that the resonance condition can be satisfied for much larger round-trip phase offsets $\Delta\phi_q$ because within the round-trip resonator propagation time, the modulation term oscillates between negative and positive β (that is, $-\beta < \beta\sin(2\pi f_m t) < \beta$).

This effect may be understood by plotting the total transmission of the EO comb generator for various β, as shown in the right inset of Fig. 2b. The transmission is calculated by averaging the output power of a time-domain representation of the electric field given in equation (3). The optical power output depends primarily on the interference between the input optical field and the optical field inside the resonator. As in a microresonator without EO modulation, the dips in the transmission spectrum correspond to a large built-up field inside the resonator. For various values of β, the width of the resonance increases, indicating that for large modulation indices, the resonance condition can be satisfied for various detuning values. As shown in Fig. 2b, the amount of detuning is approximately equal to the modulation index β, as is predicted by the phase model when $\Delta\phi_q = \phi_{\text{opt}}$.

We can now determine the contributions to the optical phase offset $\Delta\phi_q$ as a function of frequency. The optical phase offset, as discussed above, does not induce frequency-dependent phase shifts. However, microwave signal detuning and dispersion effects are frequency dependent.

Once the resonator has reached steady state, the output field is an EO comb spaced at the modulation frequency f_m, such that the qth comb line frequency is $f_q = f_0 + qf_m$. A mismatch between the microwave frequency and the resonator free spectral range, Δf_m, results in a frequency-dependent phase offset $\phi_{\text{micro}}(q) = 2\pi q \Delta f_m T$.

For an arbitrary dispersion profile, it is possible to find the frequency-dependent phase offset by integrating the group velocity dispersion profile of the waveguide. However, if the dispersion is approximately linear with frequency, the dispersion-related phase offset is $\Delta\phi_{\text{disp}}(q) = 2\pi(qf_m)^2\beta_2 L$ where $\beta_2 L$ is the round-trip group velocity dispersion in units of femtoseconds squared per millimetre.

To first order, we then have a model for the total phase offset as a function of frequency, $\Delta\phi_q = \Delta\phi_{\text{opt}} + \Delta\phi_{\text{micro}}(q) + \Delta\phi_{\text{disp}}(q)$. In fact, this model agrees exactly with the analytical model for the output comb shape developed in ref. [12]. In the case of maximum comb bandwidth, corresponding to zero microwave detuning and optical detuning satisfying $\phi_{\text{opt}} + \beta = 0$, the maximum dispersion-limited bandwidth is $\Delta f_{\text{comb}} = \frac{1}{\pi}\sqrt{\frac{2\beta}{\beta_2 L}}$, in good agreement with the results presented in ref. [29]. The bandwidth differs by up to a factor of $\sqrt{2}$ due to the difference in FSR of a Fabry–Pérot resonator and ring resonator of identical length[29].

Using this model, it is a straightforward optimization problem to start with the frequency-dependent round-trip resonance condition and alter the optical and microwave detuning so that the resonance condition is satisfied only for a desired frequency region, as is done to demonstrate the one-sided comb in Fig. 3c.

Data availability

The datasets generated and analysed during the current study are available from the corresponding authors on reasonable request.

34. Zhang, M., Wang, C., Cheng, R., Shams-Ansari, A. & Lončar, M. Monolithic ultra-high-Q lithium niobate microring resonator. *Optica* **4**, 1536–1537 (2017).
35. Wang, C., Zhang, M., Stern, B., Lipson, M. & Lončar, M. Nanophotonic lithium niobate electro-optic modulators. *Opt. Express* **26**, 1547–1555 (2018).
36. Kobayashi, T., Sueta, T., Cho, Y. & Matsuo, Y. High-repetition-rate optical pulse generator using a Fabry–Perot electro-optic modulator. *Appl. Phys. Lett.* **21**, 341–343 (1972).
37. Saitoh, T. et al. Modulation characteristic of waveguide-type optical frequency comb generator. *J. Lightwave Technol.* **16**, 824–832 (1998).
38. Kim, J., Richardson, D. J. & Slavík, R. In *2016 IEEE Photonics Conference (IPC)* 503–504, https://doi.org/10.1109/IPCon.2016.7831201 (2016).

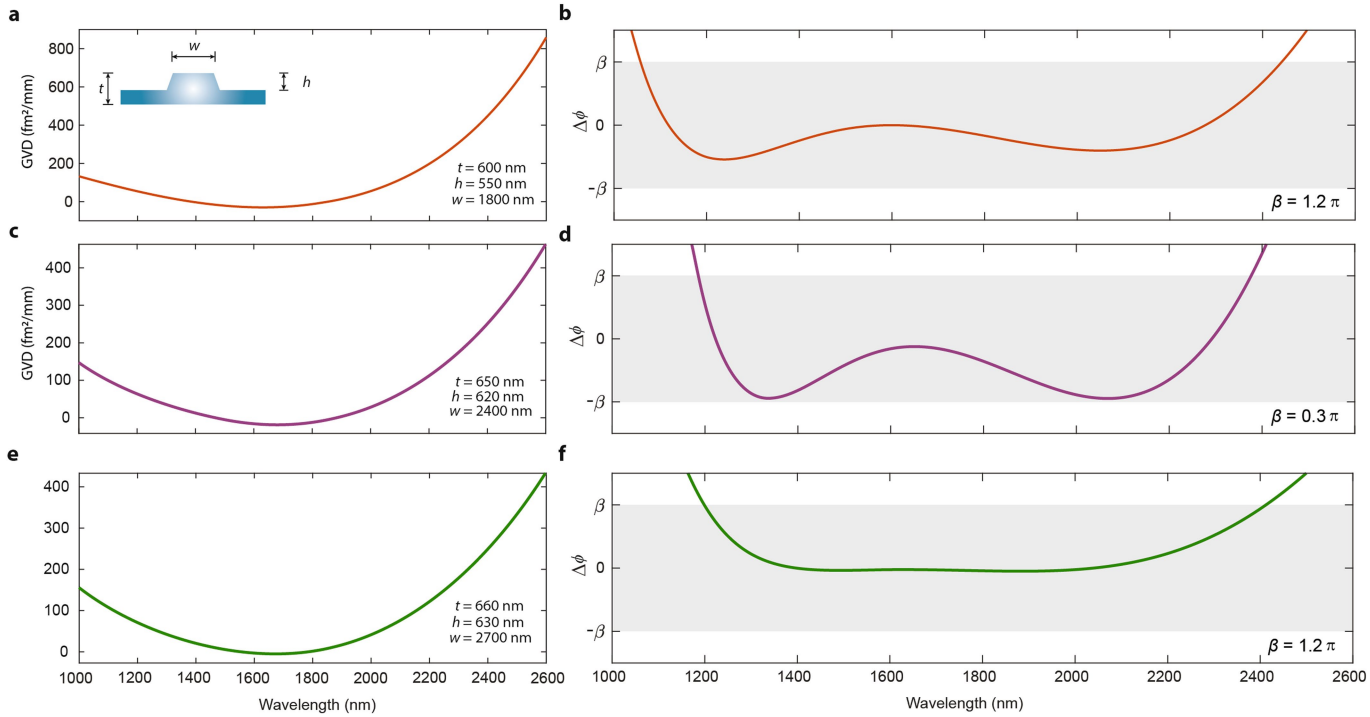

Extended Data Fig. 1 | Dispersion engineering and tailored EO comb phase-matching condition. a, Simulated dispersion for an air-clad lithium niobate ridge waveguide with top width $w = 1{,}800$ nm, film thickness $t = 600$ nm and etch depth $h = 550$ nm. **b**, The phase-matching condition for generating EO comb sidebands. The grey area shows the region of phase matching, with round-trip modulation strength β. With a 50-GHz microwave drive and $\beta = 1.2\pi$, an EO comb spanning 1.3 octaves can be generated. **c**, Simulated group velocity dispersion (GVD) for an air-clad lithium niobate waveguide with a different geometry optimized for an octave-spanning comb with small microwave driving amplitude. **d**, An octave-spanning EO comb is shown with $\beta = 0.3\pi$. **e**, Another example of an air-clad lithium niobate waveguide with dispersion engineered for broad comb generation. **f**, Such EO comb generation features a flat response over 600 nm. A broad comb spanning less than an octave can be generated in devices with small microwave modulation amplitudes and high-Q optical resonators.